RSC Advances

PAPER

Cite this: *RSC Adv.*, 2018, **8**, 21369

Study on montmorillonite–chlorhexidine acetate–terbinafine hydrochloride intercalation composites as drug release systems

Baohong Sun,[ab] Ming Zhang,[ab] Ninglin Zhou,[*abc] Xiaohong Chu,[ab] Ping Yuan,[ab] Cheng Chi,[ab] Fan Wu[ab] and Jian Shen*[ab]

This paper focuses on the intercalation of chlorhexidine acetate (CA) and terbinafine hydrochloride (TBH) into montmorillonite as sustained release drug carriers. The intercalation compounds were characterized by X-ray diffraction (XRD), Fourier transform infrared (FT-IR) spectroscopy, and thermogravimetric analysis (TGA). The basal spacing of montmorillonite increased from 1.23 to 2.97 nm. It was confirmed that CA and TBH molecules were well-stabilized in the interlayer space of clay *via* mono-, double or triplicate layer stacking. The adsorption amounts and molecular structures of CA and TBH appeared to depend on the cation exchange capacity of MMT, which in turn, tailored the drug release patterns. *In vitro* release tests of MMT–CA–TBH in 0.9 wt% NaCl solution at 37 °C show a biphasic and sustained profile of CA and TBH ion release. After release, dissolution–diffusion kinetic models were fitted. The mechanism of MMT–CA–TBH release is probably due to surface diffusion and bulk diffusion *via* ionic exchange of MMT ions on or in the MMT with ions in the NaCl solution. The *in vitro* release experiments revealed that CA and TBH were released from MMT steadily, depending on the cooperation between the drugs themselves and the electrostatic interactions between the drugs and MMT. It was found that the cross-linking ratio increased due to a decrease in the free volume available for diffusion.

Received 27th April 2018
Accepted 17th May 2018

DOI: 10.1039/c8ra03651a

rsc.li/rsc-advances

1. Introduction

Nowadays, antimicrobial materials are widely used in our daily life due to their suitability for public health protection.[1] Materials with antimicrobial properties are capable of inhibiting the growth of, or even killing, certain kinds of microorganisms such as bacteria or fungi. The increase in emergence and re-emergence of multidrug-resistant pathogens especially antibiotic-resistant bacterial strains, fungi, and parasites, has become a serious problem in the health care and food technology sectors.[2,3] Extensive use of antimicrobial agents contributes to the development and rapid spread of bacterial resistance, which implies a decrease in antibiotic efficacy in both human and veterinary medicine. Microbes acquire resistance to various drugs to shield themselves against all odds and develop favorable modifications to enable their comfortable survival and multiplication under extreme conditions.[4,5] Safety concerns associated with the drug-resistant microbes and continuing emphasis on health care costs have stressed the need for modifications to traditional antimicrobial compounds or research into other promising alternatives. New resistance mechanisms, such as enzymes destroying antibiotics, have emerged, making the new generation of antibiotics virtually ineffective. Therefore, various inorganic and organic antimicrobial materials have been intensively investigated to resolve the problem of microbial contamination.[6,7]

Inorganic nanoparticles have a positive effect on killing strains such as Gram-negative bacteria, Gram-positive bacteria and fungi.[8] Their main advantages are stability and a long shelf life compared with organic antibacterial agents. Nanostructured metallic particles have emerged as powerful tools over the last two decades, displaying an array of unprecedented physiochemical and optoelectronic properties.[9] In particular, noble metal nanostructures, such as silver nanoparticles, exhibit unique and tunable surface plasmon properties, ease of surface functionalization, extremely high surface to volume ratios, and catalytic effects in many important oxidization reactions.[10] These characteristics promote their broad functions in diverse applications ranging from targeted drug delivery and molecular imaging to antimicrobial development.[11] However, despite the ease of such fabrication methods and their reliability in creating a complex morphology of silver nanoparticles, toxicity and biocompatibility concerns have severely impeded their application in critical domains, *e.g.*, in healthcare theranostics.[12]

[a]*Jiangsu Collaborative Innovation Center for Biological Functional Materials, College of Chemistry and Materials Science, Nanjing Normal University, Nanjing 210023, China. E-mail: zhouninglin@njnu.edu.cn*

[b]*Jiangsu Key Laboratory of Biofunctional Materials, Jiangsu Engineering Research Center for Biomedical Function Materials, Nanjing 210023, China*

[c]*Nanjing Zhou Ninglin Advanced Materials Technology Company Limited, Nanjing 211505, China*

In consequence, the development of materials capable of inhibiting bacterial growth in connection with the controlled administration and distribution of antibacterial substances has attracted great interest in recent years. Much of this attention has been attracted by clays, zeolites, and other aluminosilicates which have been used successfully as carriers of antibacterial substances loaded into a ceramic matrix by ion exchange. The specific layered structure and high ion exchange capacity of aluminosilicates are accompanied by high surface area development and sorptive capacity, a negative surface charge, chemical inertness, and low or even no toxicity, and this makes them particularly attractive for this type of application.[13,14] Some studies have even revealed that clays can absorb bacteria such as *Escherichia coli* and *Staphylococcus aureus* and immobilize cell toxins.[15] Other researchers found, however, that natural clay minerals showed no antibacterial effect, but were able to absorb and kill bacteria only when substances characterised by antimicrobial activity were intercalated.[16,17]

Montmorillonite (MMT), a kind of layered aluminosilicate, is composed of tetrahedral sheets of SiO_4 units and octahedral sheets of Al^{3+} ions. The isomorphous substitution of Al^{3+} with Mg^{2+} or Fe^{2+} in octahedral sheets or that of Si^{4+} with Al^{3+} in tetrahedral ones can generate negative surface charge. MMT possesses hydrophilicity, high dispersibility in water, and most importantly, cation exchange capacity (CEC). The interlayer spacings in MMT are wide enough for small molecules and ions to enter, occupy and diffuse through.[18,19] On the other hand, the intercalation of guests makes the interlayer spacing even wider, resulting in lattice expansion along the direction perpendicular to the layers. So MMT can encapsulate various protonated and hydrophilic organic molecules into the interlayer spaces of the (001) plane, and these can be released in a controlled manner by replacement with other kinds of cation in the release media.[20]

A number of studies have focused on the interaction of guest molecules with clays including MMT. Rapacz-Kmita *et al.* studied the synergistic antibacterial activity and slow drug release of montmorillonite and gentamicin;[21] Saha *et al.* studied the inhibition of *E. coli* and *S. aureus* by chlorhexidine acetate–montmorillonite composites;[22] Ambrogi *et al.* studied montmorillonite–chitosan–chlorhexidine intercalated films with antimicrobial activity and improved toxicity for wound dressing.[23] These are all studies of antibacterial activity, but there is currently a lack of research on antifungals. Many of them are organically modified with montmorillonite and act synergistically with other substances as fungicides. Gamba *et al.* studied the interactions of the fungicide thiabendazole on montmorillonite and organoclays synthesized from phosphatidylcholine and octadecyltrimethylammonium bromide.[24] Pola *et al.* studied the active films based on cellulose acetate incorporated with different concentrations of oregano essential oil and organophilic montmorillonite clay to control the growth of phytopathogenic fungi.[25] However, there are few studies on the simultaneous inhibition of bacteria and fungi using montmorillonite intercalation.[26] The materials studied in this article can simultaneously inhibit bacteria and fungi, release drugs for a longer period of time, and effectively fill gaps in this area.

CA is a biguanide antiseptic and disinfectant which is bactericidal or bacteriostatic against a wide range of Gram-positive and Gram-negative bacteria. CA has been widely used for diminishing inflammation, disinfecting, and washing surfaces of wounds.[22,27,28] TBH is a new potent antifungal agent of the allylamine class that selectively inhibits fungal squalene epoxidase. The drug has broad-spectrum activity against yeast, fungi, molds, and dermatophytes and is indicated for both oral and topical treatment of mycosis.[29–31]

Using an intercalation-assembly method, drugs such as CA and TBH can be inserted in the planes of MMT and achieve the purpose of slowing down the release rate of drugs through the process of ion exchange. The sustained-release control agents have the following advantages: (1) the onset time is not slower than the conventional agents, and the role of the time; (2) they reduce the number of drugs, and become more cost-effective; (3) they enable a smooth drug concentration, and reduce the side effects of drugs.[32] A more detailed approach, involving assessment of the concentration/depth profile of the drug as a function of time, has also been proposed.[33] Therefore MMT is suggested to be a good delivery carrier of hydrophilic drugs. MMT and CA–TBH were employed as inorganic matrices and organic guest molecules, respectively.

In this study, MMT–CA, MMT–TBH, and MMT–CA–TBH were successfully synthesized employing three different intercalation materials, which were CA, TBH, and CA–TBH. They could be expected to enhance the encapsulation efficiency of drugs and reduce the adverse effects of drugs because the clay used in this study is able to control the drug release behavior. These three kinds of hybrids were characterized *via* powder XRD, FT-IR, and TG. The release profiles of CA, TBH, and CA–TBH were also studied by UV-vis spectrometry. Gram-negative bacteria (*Escherichia coli*, *Pseudomonas aeruginosa*), Gram-positive bacteria (*Staphylococcus aureus*), and fungi (*Candida albicans*), very common microorganisms, were chosen to investigate the antimicrobial activities of the modified material. The preparation process of MMT–CA–TBH and its antimicrobial properties are shown in Fig. 1.

2. Materials and methods

2.1. Chemicals

CA was kindly supplied by Aide Acridine Chemical Plant (Jintan, China). TBH was provided by Z.K.T.D Drug Co., Ltd (Shandong, China) and used as received. MMT (MMT-Na) was from Zhejiang Clay Minerals Co., China. Deionized water (Millipore Milli-Q grade) with a resistivity of 18.2 MΩ was employed in all experiments. All other reagents were analytical grade.

2.2. Preparation of MMT–CA–TBH

Prior to the preparation of samples for testing, the cation exchange capacity (CEC) of MMT was determined using the method developed by Meier and Kahr,[34] using copper(II) triethylenetetramine. On this basis, the CEC of MMT = 45.4 ± 1.4 mmol per 100 g. Knowledge of the CEC of smectite and the molar mass of gentamicin sulfate enabled us to calculate the

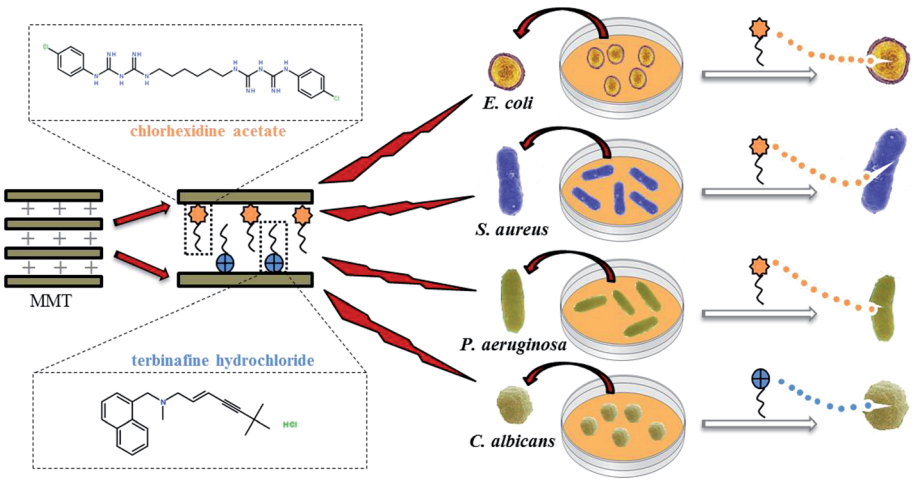

Fig. 1 Schematic representation of the synthesis of antimicrobial composite MMT–CA–TBH and its inhibitory effects on bacteria and fungi.

optimum amount of medication which could be intercalated between the layers of MMT using the formula:

$$\mathrm{CEC} = \frac{x}{100} \times \frac{y}{z} \times \frac{M}{1000}$$

where CEC – cation exchange capacity (mmol g^{-1}), x – the amount of modifying agent (g), y – assumed amount of aluminosilicate (g), z – adsorption cation valence, and M – molar mass of the modifying agent (g mol^{-1}).

Various amounts of CA (or TBH or MMT–CA) were added to 60 mL 1 wt% ultrasonically dispersed MMT, and stirred at 80 °C for 3 h. Then the mixture was filtrated through a 0.45 μm membrane filter to remove the floating small MMT particles. Finally, the mixture was dialyzed through a 500–1000 Da dialysis membrane in 1 L ultrapure water with vigorous stirring and then recharged with fresh medium every 24 h over the course of 72 h. The resultant MMT–CA–TBH solution was lyophilized to obtain the dry MMT–CA–TBH product. The sediment was dried in a vacuum oven and ground for XRD, FT-IR, and TGA characterization.

2.3. XRD

The XRD analysis was performed in the range of $0.1 < 2\theta < 10$ with CuKα radiation using a Rigaku DMAX-RC diffractometer (Japan) at 3 °C min^{-1}. The analysis was focused on the range of $3 < 2\theta < 10$, where most characteristic diffraction peaks were expected.

2.4. FT-IR

The FTIR spectra were recorded using a FTS 3000 Excalibur spectrometer in the range of 400 to 4000 cm^{-1}, with a resolution of 4 cm^{-1}. The powders, in amounts of 2 mg, were mixed thoroughly in an agate mortar with 100 mg KBr and moulded into the form of pastilles in a hydraulic press.

2.5. TGA

TGA was performed using a 7-series Thermogravimetric Analyzer produced by Perkin-Elmer, USA. The test conditions were as follows: high purity nitrogen atmosphere, heating rate 20 °C min^{-1}, and air flow rate 50 mL min^{-1}.

2.6. Drug release test

The dissolution test was performed using a shaker bath (SV1422, Schutzart, Germany) by suspending dialysis bags containing MMT–CA (or MMT–TBH or MMT–CA–TBH) in 200 mL of 0.9 wt% NaCl solution at 37 °C. At suitable intervals, 5 mL of the dissolution medium was taken and the CA content (or TBH or CA–TBH, respectively) was determined by UV absorption at λ_{max} (CA: 260 nm; TBH: 282 nm). The same dissolution medium was immediately refilled and the volume was maintained at 200 mL.[35] Tests were made in triplicate and the results were recorded as averages.

2.7. Disk diffusion test

The microorganism resistance of MMT-Na and MMT–CA–TBH were evaluated against Gram-positive, Gram-negative bacteria, and fungi using a disk diffusion test (ATTCC 90: 2011). 0.1 g of MMT–CA–TBH composite powder and 0.1 g of MMT powder were compressed into 13 mm diameter discs, with three samples per strain, averaged, and steam sterilized at a pressure of 0.1 MPa for 20 minutes. *S. aureus* (ATCC 25923), *E. coli* (ATCC 25922), *P. aeruginosa* (ATCC 27853), and *C. albicans* (ATCC 10231) were cultured in a broth medium at 37 °C for 24 h to prepare a microorganism suspension and then used. The prepared agar medium was taken and poured into the plate (10–15 mL), and solidified for use. 0.5 mL of the microorganism suspension was aspirated into 150 mL agar medium cooled to about 45 °C with a sterile pipette, and the microorganism suspension was thoroughly and uniformly dispersed on the melted agar medium. It was then injected into a solidified, uniform, low-level agar medium (10–15 mL), and shaken immediately to condense naturally. The sterilized sample was placed in the middle of the agar plate, and then the remaining sample was placed in the same direction as the time direction, and it was gently compacted so that the sample was in full contact with the plate, but without

Table 1 The results of the layer spacings of MMT with different intercalations

Sample	d_{001}apex2θ/(deg.)	d (nm)
MMT-Na	5.32	1.53
MMT–CA = 3 : 1 (w/w)	4.53	1.93
MMT–TBH = 2 : 1 (w/w)	3.16	2.79
MMT–CA–TBH = 3 : 2 : 2 (w/w)	3.54	2.49

destroying the surface of the culture medium, then the sample was inverted. The agar plate was placed in a constant temperature incubator at 37 °C for 48 h and observed for the presence of the zone of inhibition (Table 1).

3. Results and discussion

3.1. XRD analysis

In our previous work, we have proven that the basal spacing of MMT–CA reached a plateau at 1.93 nm when the ratio of CA : MMT was adjusted to 3 : 1 (wt%),[16] while the basal spacing of MMT–TBH reached a plateau at 2.79 nm when the ratio of TBH : MMT was adjusted to 2 : 1 (wt%). However, the basal spacing of MMT–CA–TBH reached a plateau at 2.49 nm, which is wider than the former and narrower than the latter when the ratio of CA : TBH : MMT was adjusted to 3 : 2 : 2 (wt%). It seems that the interaction between CA and TBH has an effect on the spacing of MMT. Therefore, the structure of CA–TBH in the layers of MMT was further studied (Table 2).[36]

The height of a CA molecule is 0.5 nm, computed from the structure of CA (Fig. 3a and b). According to the crystal structure of MMT, its thickness of two layers is 0.97 nm, so the height of the space is 0.54 nm when the ratio of CA : MMT is 3 : 1 (wt%), corresponding with the height of a CA molecule (Fig. 3a). It became evident that CA molecules in the MMT interlayer (CA : MMT = 3 : 1) were stabilized in a double layer arrangement. This is surely due to the large CEC of MMT.[18] In the same way, TBH molecules in the MMT interlayer (TBH : MMT = 2 : 1) were stabilized in a triplicate layer arrangement (the height of TBH is 0.87 nm). But the situation changed when both CA and TBH were successfully intercalated in the layers of MMT (CA : TBH : MMT = 3 : 2 : 2), as the space of the layer is only 2.49 nm. It is suggested that the structures of both CA and TBH were different from the initial crystal structures and an unknown molecular interaction existed between them.[35] This is confirmed by the results of FT-IR and later, the drug release model.

Table 2 The bond length of different bond participants

Bond participants	Bond type	Bond length (nm)
A carbon and a hydrogen atom	Single	0.108
Two sp^3 carbon atoms	Single	0.154
Two sp^2 carbon atoms	Double	0.140
Two sp carbon atoms	Triple	0.118

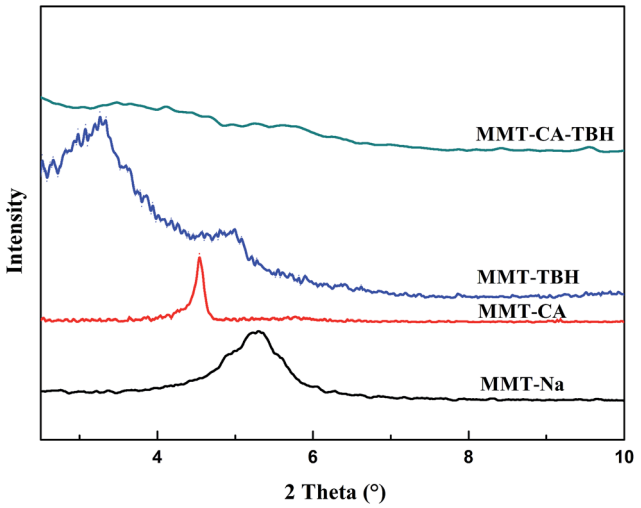

Fig. 2 XRD of MMT-Na, MMT–CA, MMT–TBH, and MMT–CA–MMT intercalates.

3.2. FT-IR spectra analysis

FT-IR spectroscopy is a useful technology to investigate the microstructures and surface properties of clays and related materials. The FT-IR spectra of MMT–CA, MMT–TBH, and MMT–CA–TBH are shown in Fig. 4. The FT-IR spectrum of MMT shows the characteristic absorption bands at 1043, 932, and 482 cm^{-1}. For CA, sharp peaks corresponding to the C=O stretching, C–H wagging, and C=N stretching bands were observed at 1697, 1313, and 1498 cm^{-1}, respectively.[37] The stretching vibrations of sp^3 C–H were also seen at 2926 and 2856 cm^{-1}. All of these characteristic bands were also clearly shown in the spectra of the hybrids, indicating that CA molecules were well-stabilized in the interlayer spaces of clay without any chemical deterioration of the functional groups.[38] It was found that the FT-IR spectra of all of the samples displayed a band at 3620 cm^{-1}, corresponding to the O–H stretching vibration of the structural hydroxyl groups. The IR spectra of the three series of resulting samples are similar to that of MMT. However, there is a difference between those of raw MMT and the resulting samples. After the intercalation of CA, the absorption band at 3420 cm^{-1} corresponding to the symmetric ν(O–H) stretching vibration band of adsorbed water shifts to a higher frequency at 3483 cm^{-1}, reflecting a decrease in adsorbed water on the external surface or in the interlayer spaces of MMT. This suggests that the hydrophilicity of the MMT surface decreases and the hydrophobic properties increase after the intercalation of CA.[39] In addition, the absorptions at 3380 and 3230 cm^{-1} are attributed to the N–H and C–H stretching vibrations of the aromatic ring of CA and those at 2859 and 2934 cm^{-1} to the symmetric and asymmetric stretching vibrations of the methylene groups of CA. The absorption bands in the region of 1200–1600 cm^{-1} also resulted from C–N and C–C vibrations of CA.[38] Here, it can be seen that the FTIR spectra of MMT and the resulting compounds provided complementary indications that CA has been intercalated into the MMT interlayer spaces and the hydrophilic

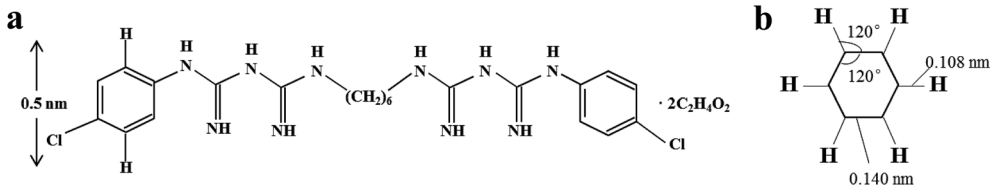

Fig. 3 The configuration of (a) chlorhexidine acetate, and (b) benzene.

surface of MMT was changed to a hydrophobic one after the intercalation of CA. This transformation can enhance the affinity of the organic antibacterial compounds towards bacteria.

The area of the TBH peak was normalized with respect to the areas under the amide I (1645 cm^{-1}) and amide II (1545 cm^{-1}) bands originating from the carbonyl stretching and the N–H bending vibrations.[40]

It should also be noted that the shifts in the C=O stretching bands could be seen upon intercalation of CA–TBH into the clay. The ν(C=O) stretching bands of CA in MMT were shifted from 1640 to 1630 cm^{-1}, which was due to the fact that the intermolecular interactions between crystallized drug molecules were absent upon hybridization. This result proved that CA molecules intercalated in the interlayer spaces were not crystallized but resided in their molecular form.[41] It was the same for MMT–TBH and MMT–CA–TBH. Not all characteristic bands belonging to MMT, CA, and TBH appear in the spectrum of MMT–CA–TBH, and several new absorption bands at 2230 and 2980 cm^{-1} are also recognized. This also indicates that CA–TBH interacts strongly with MMT layers.

3.3. TGA analysis

Fig. 5 shows the TGA profiles of the hybrids, which provides the information on the molecular arrangement and organic content in the clay lattices. The TGA curves of MMT show two distinct steps. The first one of about 7% at 48–120 °C is due to the free water evaporation. The second weight loss at 550–720 °C is due to the structural dehydration.[42]

The TGA curve of MMT–CA–TBH shows a sharp weight loss at around 200.29 °C (the first decomposition temperature) due to the decomposition of intercalated MMT–CA. This weight loss around 200.29 °C does not appear in the curve of MMT and the first decomposition temperature is between that of single MMT–CA (218.0 °C) and MMT–TBH (192.5 °C). This indicates that the thermal stabilities of CA and TBH were improved through hybridization.

Based on those decompositions, the amount of CA in MMT–CA was about 32.6% and the amount of TBH in MMT–TBH was about 20%, while the total amounts of CA and TBH in MMT–CA–TBH were found to be about 19% and 20%, respectively. The larger encapsulated amount in the MMT could be explained by the molecular arrangement of the CA and TBH in the interlayer spaces.[43] As shown in the powder XRD patterns (Fig. 2), the double layer arrangement was highly probable with MMT–CA, the triplicate layer arrangement with MMT–TBH, and the unknown layer arrangement with MMT–CA–TBH, which suggested that the drug could be encased more than those in the single intercalation system. The drugs crystallized on the surface of MMT were ignored in the TGA curves.

3.4. *In vitro* drug release

In contrast with MMT–CA and TBH–MMT, MMT–CA–TBH powder had a burst release of 35% within the first 24 h (as some CA–TBH molecules weakly electrostatically interacted with the surface of the MMT particles), followed by a steady decline of CA–TBH in solution, with only 50% of CA–TBH in solution after

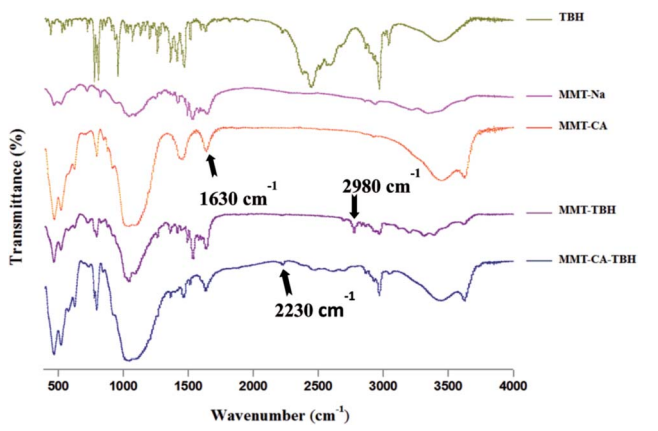

Fig. 4 FTIR spectra of TBH, MMT-Na, MMT–CA, MMT–TBH, and MMT–CA–TBH complexes.

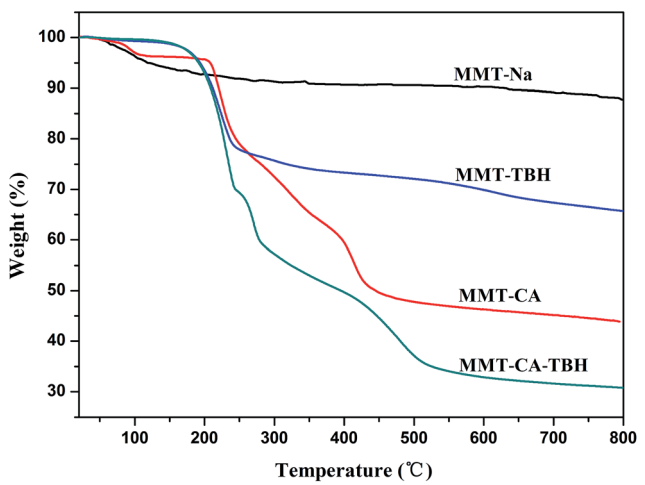

Fig. 5 TGA of MMT-Na, MMT–CA, MMT–TBH, and MMT–CA–TBH.

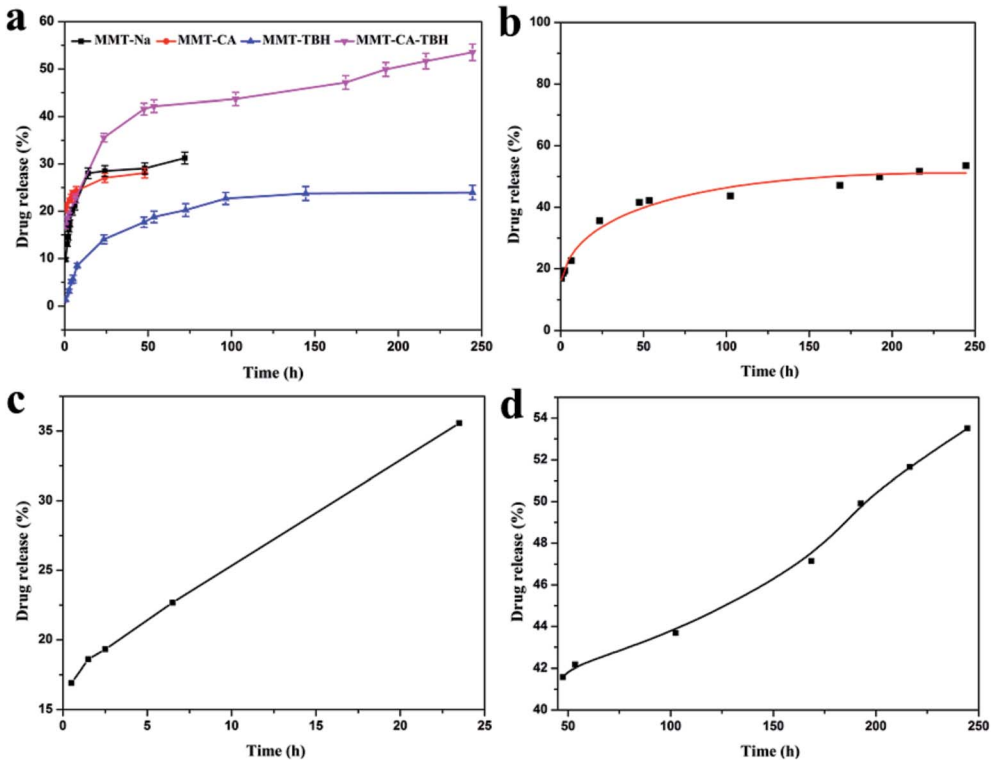

Fig. 6 (a) *In vitro* drug release curves from MMT-Na, MMT–CA, MMT–TBH, and MMT–CA–TBH. (b) *In vitro* drug release curves from MMT–CA–TBH, where the curve represents the modified parabolic diffusion model prediction. (c) *In vitro* drug release curves from MMT–CA–TBH in the first 24 h, where the curve represents the modified linear diffusion model prediction. (d) *In vitro* drug release curves from MMT–CA–TBH after 24 h, where the curve represents the modified parabolic diffusion model prediction.

40 h. The change in the release amount and release tendency from different drugs was observed as shown in Fig. 6a. When CA and TBH are both intercalated in MMT, the release amount is not equal to that of the sum of CA and TBH released from MMT–CA and MMT–TBH, respectively. This indicates that the interaction between CA and TBH exists and the nameless join realizes the stable control of the release rate efficiently. This implies that the greater extended release period for CA–TBH to release from MMT nanohybrids is largely due to the strong electrostatic interactions between the negatively charged MMT hydroxide layers and the positively charged CA–TBH ions in MMT interlayers. Due to CA–TBH's particular structure with COO^- and NH^+ in each molecule, the drug system has much stronger electrostatic interactions with MMT hydroxide layers, and can only be released when all of the binding NH^+ and COO^- are replaced by Na^+ anions.[44]

To understand the MMT–CA–TBH release behavior, we used a different model to simulate the drug release process and the Korsmeyer–Peppas model was suitable (Fig. 6b) with a linear correlation coefficient of $R^2 = 0.98$ ($y = P_1 \times x^{0.5} + P_2 \times x + P_3$). Though it explains the desorption of ions much better, it doesn't satisfy Fick's law. The whole release process consists of two stages and these are shown in Fig. 6c and d. Stage I at 0–24 h represents good linearity and stage II at 24–250 h shows a power relation between release and time ($Y = A + B \times X$, $R^2 = 0.998$; $y = P_1 \times x^{0.5} + P_2 \times x + P_3$, $R^2 = 0.994$). The diffusion model describes intraparticle diffusion or surface diffusion. These simulation results suggest that (i) the release at both stages is diffusion-controlled; (ii) within the first 24 h (stage I), most CA–TBH ions on the surface of MMT particles diffuse into the medium solution *via* ion exchange; and (iii) at stage II, surface diffusion is continuing, although it is no longer the controlling step; the controlling step is the CA–TBH ion diffusion from the inside to the surface of MMT particles, which takes a longer time than for stage I. This biphasic model prediction is consistent with the release process of CA–TBH from MMT nanohybrids. There is about 10–20% of CA–TBH on the surface or edge of the nanoparticles, which diffuses into solution *via* exchange with NaCl (stage I). Simultaneously, the bulk CA–TBH diffuses towards the edge/surface (intraparticle diffusion), resulting in the continuous release of CA–TBH from the nanohybrids (stage II).[45,46] Additionally, the kinetic model predictions suggest differences in the release of MMT–CA, MMT–TBH, and MMT–CA–TBH.

Ions in layers present a passive ion-exchange mechanism, where the interbedded ions exchange directly with ions in the medium. The speed and degree are controlled by concentration, charge, and action within layers of ions in the medium.[47] Due to the stronger electrostatic interactions with MMT and the intermolecular effects between CA and TBH, the structural space has changed, which in turn, facilitated the drug release rate. As a result, the initial fast release quickly allows the

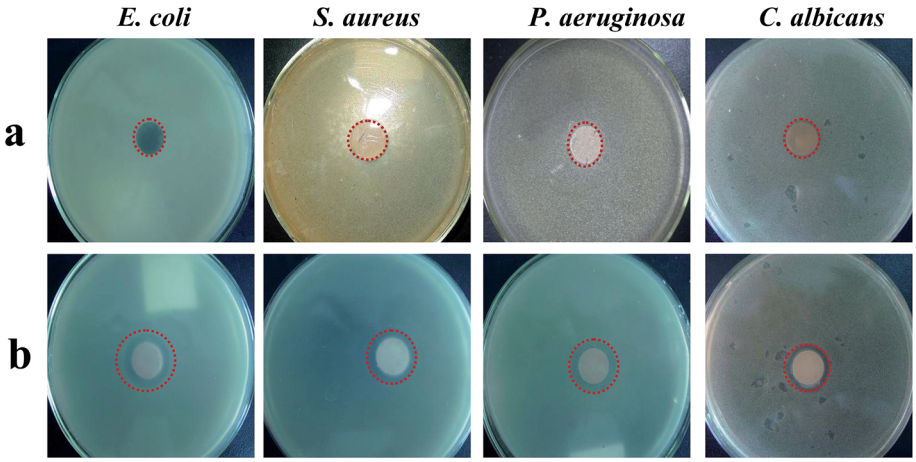

Fig. 7 Photographs showing zones of inhibition of (a) MMT-Na against *E. coli*, *S. aureus*, *P. aeruginosa*, and *C. albicans*; (b) MMT–CA against *E. coli*, *S. aureus*, and *P. aeruginosa*; MMT–CA–TBH against *C. albicans*.

Table 3 Diameters of zones of inhibition of MMT-Na and MMT–CA–TBH

Microorganism species	Initial diameter (mm)	MMT-Na	MMT–CA–TBH (mm)
E. coli	8.42	—	21.42
S. aureus	8.42	—	21.42
P. aeruginosa	8.42	—	21.42
C. albicans	5.34	—	18.34

establishment of a therapeutic dose, and the subsequent sustained release allows maintenance of this dose over a long period of time.

3.5. Inhibitory zone tests

The MMT–CA–TBH samples were evaluated individually for bacterial and fungal resistance against Gram-negative (*E. coli*, *P. aeruginosa*) and Gram-positive bacteria (*S. aureus*), and fungi (*C. albicans*). The results of the measurement zones of inhibition were averaged based on three test trials. The size of the swelling zone from the edge of each disc in the agar plate is expressed in millimeters (mm). As can be seen from Fig. 7 and Table 3, there is no inhibition zone around the sodium-based montmorillonite sample, but around the MMT–CA–TBH sample there is an obvious inhibition zone, indicating that MMT–CA–TBH has a significant inhibitory effect against *S. aureus*, *E. coli*, *P. aeruginosa*, and *C. albicans*.

At low concentrations, the mechanism of action of this biguanide drug is ATPase inactivation whereas at higher bactericidal concentrations, it induces damage of cytoplasmic membranes by precipitating essential proteins and nucleic acids, which is caused by the electrostatic attraction between the chlorhexidine (cation) and the negatively charged bacterial cells. After the adsorption onto the microorganism's cell wall, the drug molecule disrupts the integrity of the cell membrane and causes the leakage of intracellular components of the organisms.[48] As a result of this, the microorganisms gradually die. After chlorhexidine is inserted into MMT-Na, the surfaces of the lamellae are covered with long alkyl chains, and these cause the surfaces of montmorillonite to change from hydrophilic to lipophilic. Since the substances constituting the bacterial cell wall are mostly oleophilic substances, MMT–CA is more likely to adsorb bacteria. Compared with the MMT-Na, the surface charge of the MMT–CA antibacterial material becomes positive, and the electrostatic adsorption with negatively charged bacteria is stronger, so that the effect of inhibiting bacterial growth is enhanced. Due to the barrier effect of the montmorillonite layer, the diffusion path of the drug is increased, thereby achieving controlled release and long-term sterilization. The cell wall structures of Gram-positive bacteria and Gram-negative bacteria are very different. From the structure of the cell wall, Gram-positive bacteria have much thicker peptidoglycan cell walls than Gram-negative bacteria, but their rough structure makes it difficult to prevent the diffusion of small molecules, while the other components of the Gram-negative bacterial cell walls are more complex than those of the Gram-positive bacteria, and they have an outer membrane like a sieve.[49] Therefore, MMT–CA has the best antibacterial effect against *S. aureus*. TBH is an allylamine antifungal agent which has a bacteriostatic effect against *C. albicans*.[31] Its mechanism of action is selective inhibition of fungal squalene epoxidase, resulting in a lack of synthesis of ergosterol and accumulation of a large amount of squalene, so that the fungal cell membrane synthesis is blocked, and thus it plays a role in killing fungi.[50] Both have a good antimicrobial effect on the urinary system-controlling strains *S. aureus*, *E. coli*, *P. aeruginosa*, and *C. albicans*. This result reveals that MMT–CA–TBH can treat some diseases induced by bacteria and fungi, such as gonococcal urethritis disease. As we know, gonococcal urethritis disease is caused by the infection of *S. aureus*, *E. coli*, and *C. albicans*.[51] The disease has surpassed gonorrhea in Europe and the United States and has taken the lead among sexually transmitted diseases.[52] Most of the current cases are treated with antibiotics, but there are too many hidden dangers caused by antibiotics.[53] MMT–CA–TBH can inhibit these three

kinds of microorganism at the same time, and prolong the treatment cycle through sustained release, making it a potential material for the cure of this disease.

4. Conclusions

In summary, CA and TBH molecules were successfully intercalated by ion exchange reactions without any deterioration of their functional groups. The thermal stability of drug molecules was also improved after the hybridization. We found that the absorption amount and molecular arrangement of the drug molecules in the interlayers, as well as the release patterns of drugs, are related to the CEC of MMT itself. The *in vitro* release experiments showed that the release of CA–TBH from MMT–CA–TBH was affected by the structure of the molecules in the layers of MMT, different interactions between drugs and the binding between drugs and MMT. Overall, we have shown that MMT–CA can be stored in MMT interlayers and sustainably released under simulated body conditions.

Conflicts of interest

The authors declare no competing financial interest.

Acknowledgements

The authors gratefully acknowledge the support of this work by Jiangsu province science and technology support plan (BE2015367), the Priority Academic Program Development of Jiangsu Higher Education Institutions (PAPD) and the Jiangsu Collaborative Innovation Center of Biomedical Functional Materials.

References

1 M. Zhang, W. T. Wang, P. Yuan, C. Chi, J. Zhang and N. L. Zhou, *Chem. Eng. J.*, 2017, **330**, 1137–1147.
2 G. G. Ying, L. Y. He, A. J. Ying, Q. Q. Zhang, Y. S. Liu and J. L. Zhao, *Environ. Sci. Technol.*, 2017, **51**, 1072–1073.
3 P. Gao, S. He, S. L. Huang, K. Z. Li, Z. H. Liu, G. Xue and W. M. Sun, *Appl. Microbiol. Biotechnol.*, 2015, **99**, 3971–3980.
4 K. M. Shea, *Pediatrics*, 2003, **112**, 253–258.
5 B. M. Marshall and S. B. Levy, *Clin. Microbiol. Rev.*, 2011, **24**, 718–733.
6 WHO Antimicrobial Resistance, http://www.who.int/mediacentre/factsheets/fs194/en/, 2014.
7 S. H. Cha, J. Hong, M. McGuffie, B. Yeom, J. S. VanEpps and N. A. Kotov, *ACS Nano*, 2015, **9**, 9097–9105.
8 Y. Zhang, Q. Xu, F. Fu and X. Liu, *Cellulose*, 2016, **23**, 2791–2808.
9 S. J. Soenen, W. J. Parak, J. Rejman and B. Manshian, *Chem. Rev.*, 2015, **115**, 2109–2135.
10 W. Shao, X. Liu, H. Min, G. Dong, Q. Feng and S. Zuo, *ACS Appl. Mater. Interfaces*, 2015, **7**, 6966–6973.
11 S. Prabhu and E. K. Poulose, *Int. Nano Lett.*, 2012, **2**, 32.
12 M. Ahamed, M. S. AlSalhi and M. K. J. Siddiqui, *Clin. Chim. Acta*, 2010, **411**, 1841–1848.
13 M. I. Carretero, *Appl. Clay Sci.*, 2002, **21**, 155–163.
14 M. I. Carretero, C. Gomes and F. Tateo, *Dev. Clay Sci.*, 2006, **1**, 717–741.
15 P. Herrera, R. C. Burghardt and T. D. Phillips, *Vet. Microbiol.*, 2000, **74**, 259–272.
16 N. Meng, N. L. Zhou, S. Q. Zhang and J. Shen, *Int. J. Pharm.*, 2009, **382**, 45–49.
17 A. Phukan, R. P. Bhattacharjee and D. K. Dutta, *Adv. Powder Technol.*, 2017, **28**, 139–145.
18 G. F. Wang, S. Wang, Z. M. Sun, S. L. Zheng and Y. F. Xi, *Appl. Clay Sci.*, 2017, **148**, 1–10.
19 Y. F. Xi, Z. Ding, H. P. He and L. R. Frost, *J. Colloid Interface Sci.*, 2004, **277**, 116–120.
20 X. L. Qu, Y. J. Zhang, H. Li, S. R. Zheng and D. Zhu, *Environ. Sci. Technol.*, 2011, **45**, 2209–2216.
21 A. Rapacz-Kmita, M. M. Bućko, E. Stodolak-Zych, M. Mikołajczyk, P. Dudek and M. Trybus, *Mater. Sci. Eng., C*, 2017, **70**, 471–478.
22 K. Saha, B. S. Butola and M. Joshi, *Appl. Clay Sci.*, 2014, **101**, 477–483.
23 V. Ambrogi, D. Pietrella, M. Nocchetti, S. Casagrande, V. Moretti, S. De Marco and M. Ricci, *J. Colloid Interface Sci.*, 2017, **491**, 265–272.
24 M. Gamba, P. Kovář, M. Pospíšil and R. M. T. Sánchez, *Appl. Clay Sci.*, 2017, **137**, 59–68.
25 C. C. Pola, E. A. A. Medeirosa, O. L. Pereirab, V. G. L. Souzaa, C. G. Otonia, G. P. Camillotoa and N. F. F. Soaresa, *Food Packaging and Shelf Life*, 2016, **9**, 69–78.
26 S. Jayrajsinh, G. Shankar, Y. K. Agrawal and L. Bakre, *J. Drug Delivery Sci. Technol.*, 2017, **39**, 200–209.
27 S. Holešová, J. Štembírek, L. Bartošová, G. Pražanová, M. Valášková, M. Samlíková and E. Pazdziora, *Mater. Sci. Eng., C*, 2014, **42**, 466–473.
28 C. Chi, B. H. Sun, N. L. Zhou, M. Zhang, X. H. Chu and P. Yuan, *Colloids Surf., B*, 2018, **163**, 301–308.
29 N. I. Elsherif, R. N. Shamma and G. Abdelbary, *AAPS PharmSciTech*, 2017, **18**, 551–562.
30 N. Çelebi, S. Ermiş and S. Özkan, *Drug Dev. Ind. Pharm.*, 2015, **41**, 631–639.
31 S. M. AbdelSamie, A. O. Kamel, O. A. Sammour and S. M. Ibrahim, *Eur. J. Pharm. Sci.*, 2016, **88**, 91–100.
32 R. I. Liescu, E. Andronescu, C. D. Ghitulica, G. Voicu, A. Ficai and M. Hoteteu, *Int. J. Pharm.*, 2014, **463**, 184–192.
33 C. Herkenne, A. Naik, Y. N. Kalia, J. Hadgraft and R. H. Guy, *J. Invest. Dermatol.*, 2007, **127**, 135–142.
34 P. M. Lorenz, *Clays Clay Miner.*, 1999, **47**, 386–388.
35 Z. Gu, A. C. Thomas, Z. P. Xu, J. H. Campbell and G. Q. Lu, *Chem. Mater.*, 2008, **20**, 3715–3722.
36 J. K. Park, Y. B. Choy, J. M. Oh, J. Y. Kim, S. J. Hwang and J. H. Choy, *Int. J. Pharm.*, 2008, **359**, 198–204.
37 M. Zhang, W. T. Wang, F. Wu, P. Yuan, C. Chi and N. L. Zhou, *Carbon*, 2017, **123**, 70–83.
38 D. Yang, P. Yuan, J. X. Zhu and H. P. He, *J. Therm. Anal. Calorim.*, 2007, **89**, 847.
39 D. M. Chen, J. Chen, X. L. Luan, H. P. Ji and Z. G. Xia, *Chem. Eng. J.*, 2011, **171**, 1150–1158.
40 P. Thatai and B. Sapra, *Ther. Delivery*, 2018, **9**, 99–119.

41 F. J. Rodríguez, L. A. Cortés, A. Guarda, M. J. Galotto and J. E. Bruna, *J. Mater. Sci.*, 2015, **50**, 3772–3780.
42 K. Cheng and Z. Heidari, *Appl. Clay Sci.*, 2017, **143**, 362–371.
43 P. Huang, X. Zhao and L. Ye, *Composites, Part B*, 2015, **83**, 134–141.
44 M. L. Bello, A. M. Junior, B. A. Vieira, L. R. Dias, V. P. de Sousa, H. C. Castro, C. R. Rodrigues and L. M. Cabral, *PLoS One*, 2015, **10**, e0121110, DOI: 10.1371/journal.pone.0121110.
45 M. Makaremi, K. D. Jordan, G. D. Guthrie and E. M. Myshakin, *J. Phys. Chem. C*, 2015, **119**, 15112–15124.
46 V. Bizovská, Ľ. Jankovič and J. Madejová, *Appl. Clay Sci.*, 2018, **158**, 102–112.
47 H. Tan, B. Gu, B. Ma, X. Li, C. Lin and X. Li, *Appl. Clay Sci.*, 2016, **129**, 40–46.
48 T. Kuyyakanond and L. B. Quesnel, *FEMS Microbiol. Lett.*, 1992, **100**, 211–215.
49 T. Proft and E. N. Baker, *Cell. Mol. Life Sci.*, 2009, **66**, 613–635.
50 N. Meng, N. L. Zhou, S. Q. Zhang and J. Shen, *Appl. Clay Sci.*, 2009, **46**, 136–140.
51 J. S. Jensen, *J. Eur. Acad. Dermatol. Venereol.*, 2004, **18**, 1–11.
52 P. J. Horner, K. Blee, L. Falk, W. van der Meijden and H. Moi, *Int. J. STD AIDS*, 2016, **27**, 928–937.
53 S. O. Gose, O. O. Soge, J. L. Beebe, D. M. Nguyen, J. E. Stoltey and H. M. Bauer, *Sex. Transm. Dis.*, 2015, **42**, 279–280.